Appl Phys A (2010) 99: 197–203
DOI 10.1007/s00339-009-5496-4

**Applied Physics A**
**Materials Science & Processing**

# On the study of pH effects in the microwave enhanced rapid synthesis of nano-ZnO

**S.D. Gopal Ram · M. Anbu Kulandainathan · G. Ravi**

Received: 25 May 2009 / Accepted: 10 November 2009 / Published online: 5 December 2009


**Abstract** The rapid synthesis of ZnO nanostructures by microwave treatment of aqueous solutions of different pH values is reported for the first time. Microwave in various wattages was used as the source of heating or energy feeding the aqueous precursors. The pH of the zinc metal source was altered by a suitable amount of mineralisers. The considered pH values are 8, 10, 12 and 13.5. Microwave dielectric heating is dependent on the ability of the material to absorb microwave. This is responsible for molecular friction and dielectric loss, which as a result produce internal heating of the dielectric medium, in this case the solution. In typical microwave assisted synthesis, the total exposure to the microwave treatment was near about 25 to 35 minutes. The ZnO nanostructures obtained were studied by XRD, SEM and TEM characterisations. From the XRD pattern and the full width half maximum of the dominant reflections, microstructural parameters of the nanostructures are calculated and compared for the different pH values. Flower petal like flakes and hexagonal nanorods are formed for the lower and higher pH solutions, respectively. From the SEM images, the size distributions for the pH 12 and 13.5 cases are compared by drawing a histogram.

S.D. Gopal Ram · G. Ravi (✉)
School of Physics, Alagappa University, Karaikudi 630 003, India
e-mail: raviganesa@rediffmail.com
Fax: +91-04565-225202

M. Anbu Kulandainathan
Electro Organic Division, Central Electro Chemical Research Institute, Karaikudi 630 003, India

## 1 Introduction

Zinc oxide is one of the most attractive functional materials with unique optical and electrical properties. It is a wide band gap (3.37 eV) compound semiconductor with the exciton binding energy of 60 meV and is a promising candidate for developing high efficient ultraviolet laser device at room temperature. Thus, ZnO nanostructures have attracted considerable interest because of great potential applications in micro- and nano-optoelectronics [1, 2]. The properties of ZnO are dependent partly on the crystallinity, crystallographic orientation, crystallite size and morphology [3, 4]. Various methods such as physical, chemical, i.e., sol–gel precipitation [5, 6] methods are available for the preparation of ZnO nanostructures (ZNS). Among them, preparation from the wet chemical solution [7], hydrothermal methods are very promising and efficient in forming varieties of nanostructures such as rods, flakes, flowers etc. [8–10]. Recently the application of microwaves for heating in a hydrothermal route is drawing more attention [11–13].

In this communication, we report a rapid way of synthesising ZNS, i.e., microwave heating of the aqueous liquid precursors. Since there are two different physical mechanisms for the transfer of energy to the solutions in this case rather than in a conventional hydrothermal method, ions present in the solution can transfer energy to the solution from the microwave due to the conductive current. Another mechanism is the realignment of dipole or ion field in the alternating electric field and as a result the solution is heated. Because of this doubly internal heating method, the material coupled to the microwave field will be heated very rapidly rather here than in a convectional heating system. Here, we have studied the production of ZNS from four different solutions of varying pH from 8 to 13.5.

## 2 Experimental

0.5 g of analytical grade zinc acetate dihydrate purchased from MERCK chemicals was dissolved in 90 ml of de-ionised double distilled water. 5 ml of ammonia solution was added to the solution to increase the pH of the solution to 10, and 2 ml of ammonia was used to tune the pH to 8. In the other cases (instead of ammonia) 15, 25 ml of 2 molar NaOH solutions were added for increasing the pH of the mother solution to 12 and 13.5 respectively, and the volume of the mother liquor was varied to fill the container to a total volume of 80%. Then the solution was transferred to autoclavable Pyrex glass bottles in such a way as to fill more than 80% of the container. The container was tightly closed with a polypropylene screw cap, and the container is ready for further microwave treatment in a microwave oven, Samsung CE 1031LFB, which works with a frequency of 2.45 GHz having a maximum microwave power of 900 W. Initially the microwave oven was set in a minimum of 180 wattage of irradiation for five minutes to homogenise the solution. Then the container was exposed to 450 and 600 (for short durations) wattage of microwave radiations alternatively. Here, wattage means the intensity of radiation. Higher wattage implies that we have more intense radiation and faster heating. In the microwave oven used for the experiment, it is estimated by previous trial runs that 600 W of microwave irradiation could raise the temperature of 80 ml of the solution to 100°C in less than two minutes. The lower wattages can maintain it at lesser temperatures. To maintain the temperature inside the container within the optimum range (75–100°C), the intensity of MW radiation was reduced to 180 W for a couple of minutes and then shot up to 450 W and maintained there. For any container in hydrothermal experiments, 80% volume of filling of container is the maximum advisable and one must be cautious lest one exceed this limit.

This procedure was adopted for near about 35 minutes to let the reaction complete, and then the container was allowed to cool down naturally to the ambient. In the previous optimisation experiments, it was found that there was no effect of microwave irradiation after the saturation time limit of 35 minutes. From this we ascertain that the liquid precursors taken were exhausted off the reactants within 35 minutes of microwave irradiation. The microwave treated solution was centrifuged and the centrifugate white particles were separated and subsequently washed with ethanol and double distilled de-ionised water to remove the ionic impurities if any may be present in the ZnO powder. The filtered white slag was dried and the same was subject to X-ray diffraction analysis and scanning electron microscopy for structural and morphological analyses, respectively.

### 2.1 Principles of microwave dielectric heating

Microwave radiation produces efficient internal heating by direct coupling of microwave energy with the molecules that are present in the mixture. Microwave heats by two means of dipolar polarisation (polar solvent molecules) and ionic conduction. Upon irradiation of the microwave on a solution, the ions in the solution align in the direction of the electric field. As the applied field oscillates, the dipole or ion field attempts to realign itself with the alternating electric field, and in the process the energy is lost in the form of heat through molecular friction and dielectric loss [14, 15].

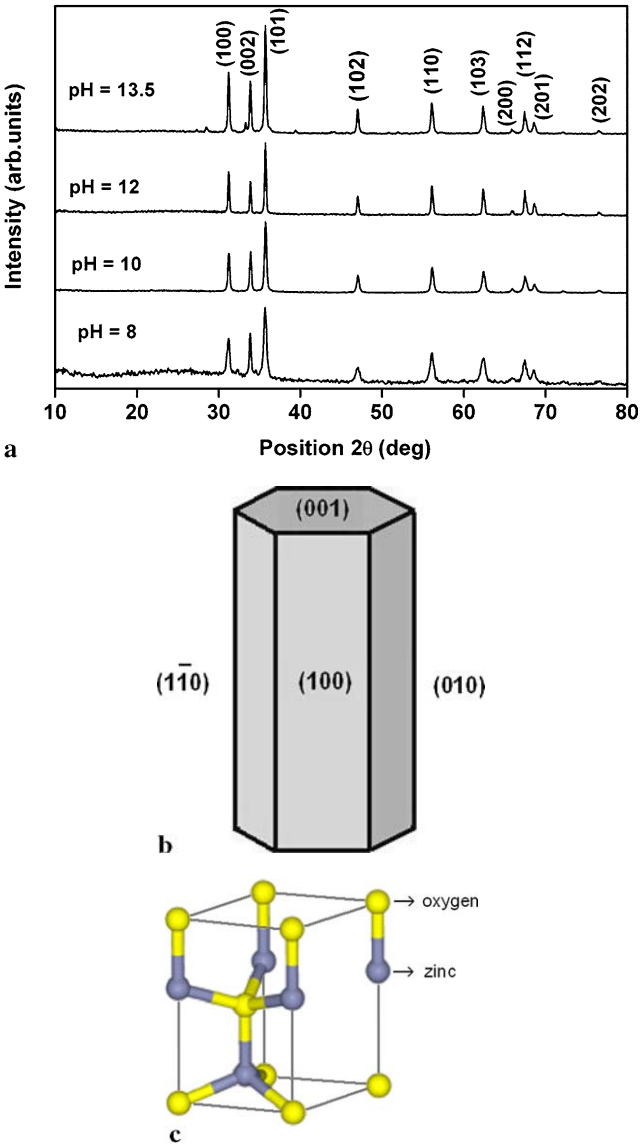


**Fig. 1** (**a**) The X-ray diffractograms of nanocrystalline ZnO, prepared by a microwave assisted hydrothermal method in the pH range of 8.5–13.5 exhibiting all of the characteristic crystalline peaks, (**b**) the hexagonal morphology of ZnO exhibiting the growth faces, and (**c**) the wurtzite structure of ZnO

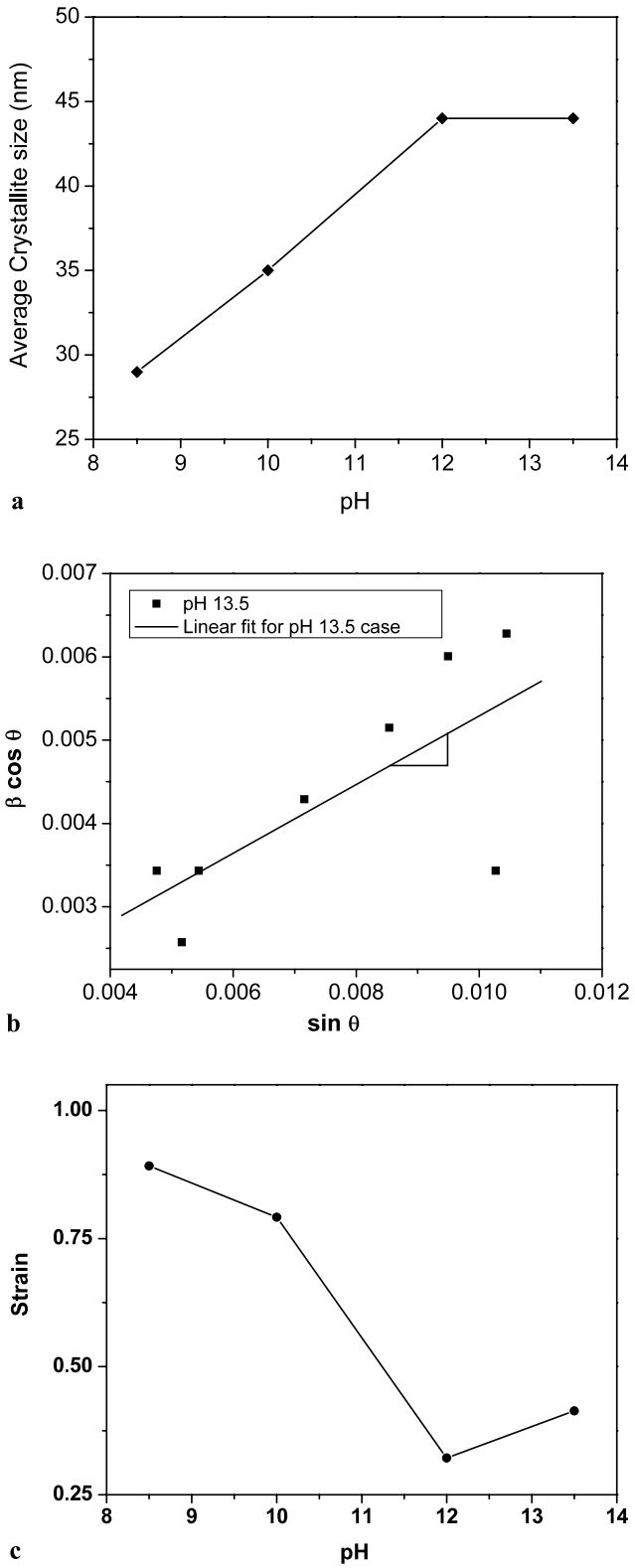


**Fig. 2** A comparison of microstructural parameters of ZnO nanostructures. (**a**) The relation of pH and grain size, (**b**) Williamson–Hall plot showing the linear fit obtained from the FWHM of ZnO prepared from the solution of pH 13.5, from the slope of which the strain is calculated, and (**c**) the variation of strain with pH as calculated from the corresponding Williamson–Hall plot

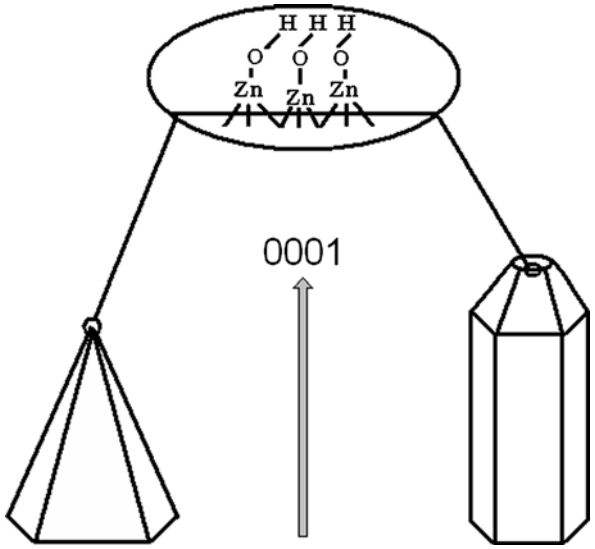


**Fig. 3** Growth habits of hexagonal prism and pyramid like ZnO crystals

Microwave heating is not intended to change the results, but to fasten the reaction process, and to reduce the reaction time from hours to minutes. In the hydrothermal process, the inability of water to deprotonate the divalent metal cations at ambient pressure, requires hydrothermal conditions [16], and the same can be achieved by conventional or microwave heating in a sealed container. According to in situ calorimetry data, dehydration of zinc hydroxide [$Zn(OH)_2$] proceeds in two stages, namely crystallisation of $Zn(OH)_2$ followed by its dissolution and recrystallisation of ZnO [17]. The total heat effect of ZnO dehydration is $8.75 \pm 0.15$ KJ/mol. In addition, in synthesis of ZnO under considerably lower temperatures than done earlier [18] it was shown that formation of ZnO takes place at 60–100°C. Hence, it is reasonable to perform synthesis of ZnO under considerably lower temperatures rather than higher temperatures. In our experiments the temperature is maintained in the range 75–100°C, which is conducive for the growth of ZnO nanostructures.

## 3 Results and discussion

### 3.1 XRD analysis

From the X-ray diffractograms, well-defined crystalline peaks of well faceted wurtzite ZnO hexagonal structure have been observed. The diffractograms were recorded by *XPERT PRO PANalytical*, Netherlands. The presence of all the characteristic peaks exhibited in Fig. 1(a) confirms that all the growth phases are grown in all the cases. The difference in the pH has shown up in the intensity of the peaks. The characteristic hexagonal morphology of ZnO indexed with the growth faces and the wurtzite structure are as presented in Fig. 1(b) and (c) respectively. For the low pH case,

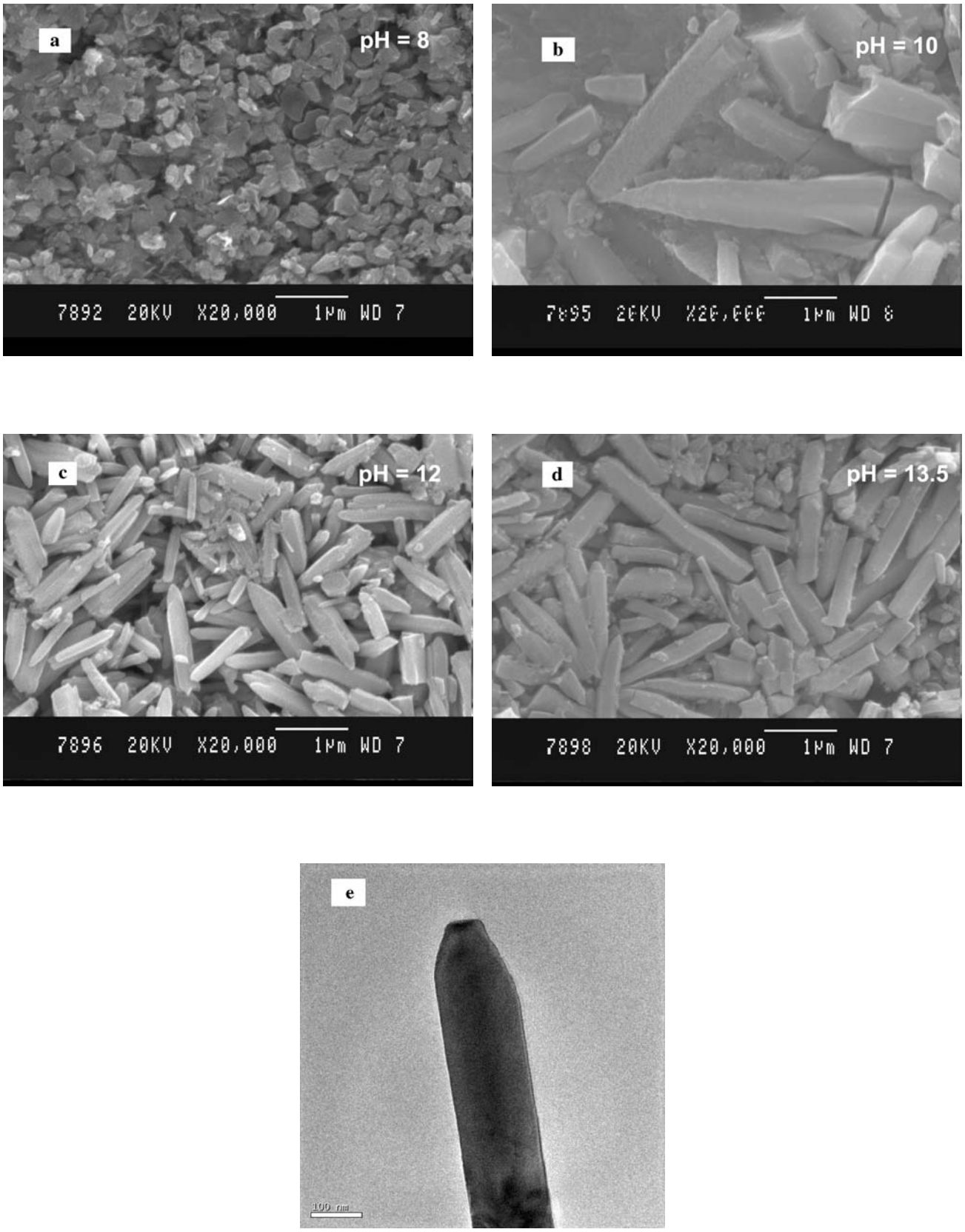


**Fig. 4** SEM images of nanocrystalline ZnO. (**a**) Nanoflakes resulting from solution of low pH 8.5, (**b**) tapered hexagonal rods yielded from pH 10, (**c**), (**d**) hexagonal ZnO nanorods produced from pH 12, 13.5 respectively, showing different numbers of size distributions, (**e**) the TEM image of a single hexagonal nanocrystal

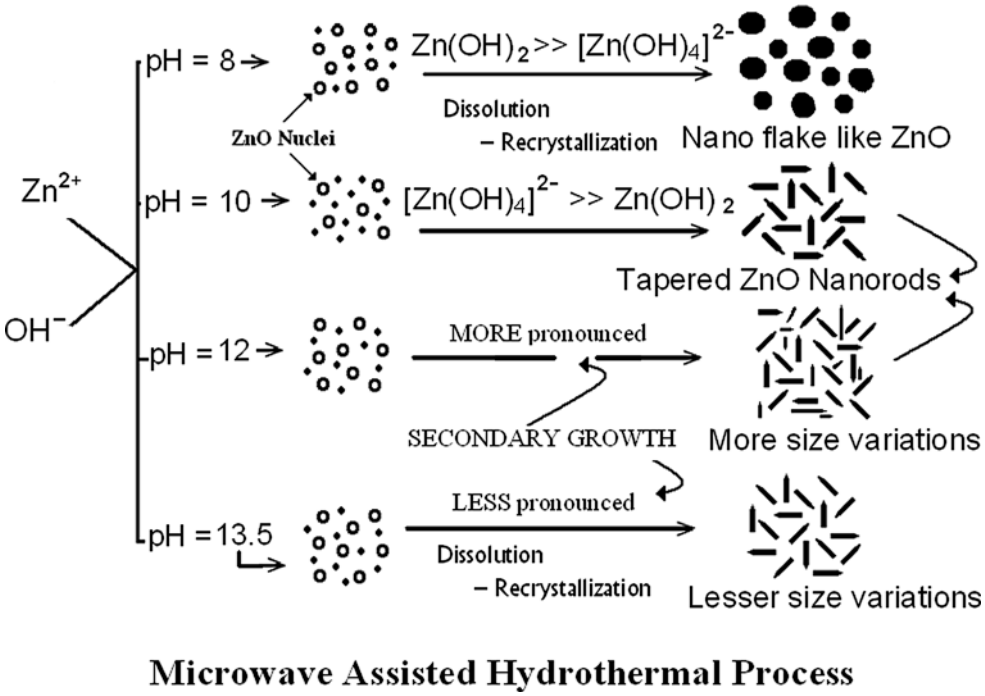


**Fig. 5** Schematic illustrating the growth phenomenon in the solutions of different pH

**Table 1** Calculated parameters of the hexagonal ZnO nanostructures prepared at different pH

| pH | FWHM ($\beta$) | Strain ($\varepsilon$) | Particle size (nm) | Lattice parameter (Å) | | Atomic packing factor ($c/a$) |
|---|---|---|---|---|---|---|
| | | | | $a$ | $c$ | |
| 8 | 0.2952 | 0.89167 | 29 | 3.3056 | 5.2947 | 1.6018 |
| 10 | 0.2460 | 0.79158 | 35 | 3.3051 | 5.2859 | 1.5993 |
| 12 | 0.1968 | 0.32200 | 44 | 3.3069 | 5.2909 | 1.5999 |
| 13.5 | 0.1968 | 0.41366 | 44 | 3.3060 | 5.2882 | 1.5996 |
| | | | | 3.249[a] | 5.206[a] | 1.6023[a] |

[a]Standard values as per JCPDS card no. 36-1451

the XRD intensity was 400 counts whereas it was 1500, 2000 and 1200 counts for pH 10, 12 and 13.5 respectively. The grain size calculated from the Scherrer formula [19, 20] shows that it increases with the increase in pH and the same is shown in Fig. 2(a).

The lattice strain of the synthesised ZNS was calculated by a Willamson–Hall plot using the formula [21]

$$\beta \cos\theta = \frac{K\lambda}{L} + \varepsilon \sin\theta \tag{1}$$

where $\beta$ is the FWHM intensity of the diffraction lines, $L$ is the crystallite size, and $\varepsilon$ the lattice strain of the ZNS, where the shape factor $K$ was assumed to be 0.89 and $\lambda$ was the wavelength of the CuK$\alpha$ radiation (1.5406 Å).

A model of the Williamson–Hall plot is shown in Fig. 2(b). The $\beta\cos\theta$ value was plotted against $\sin\theta$. The $\theta$, $\beta$ values were taken from the corresponding 100% peaks of X-ray diffraction lines. The strain is equivalent to the slope of the linear fit drawn to the plotted values. The calculated lattice strain is plotted against the pH of the initial precursor. The strain of the nanocrystals decreases with the increase in pH. This can be attributed to the increased grain size of the ascending pH of the initial precursor. The plot of strain against the pH value is presented in Fig. 2(c). In this the ZnO nanostructure formed at pH 12 shows a lowest strain compared to others. The atomic packing factors of the prepared ZNS are simulated and tabulated using their corresponding lattice parameters. All the parameters calculated above are given in Table 1. It is noteworthy that the simulated $c/a$ value is closer to the standard value for all the four different samples. The $c/a$ values of the lattice parameters of standard ASTM values in the table are denoted with an asterisk ($*$) symbol.

### 3.2 Morphological analysis and growth kinetics

Zinc oxide is a polar crystal, in which $O^{2-}$ is in hexagonal closest packing, and each $Zn^{2+}$ lies within a tetrahedral group of four oxygen ions. Zn and oxygen atoms are stacked alternatively along the $c$-axis and the top face (0001)

consists of tetrahedral zinc having a terminal OH ligand as shown in Fig. 3 (pyramid). The formation of hexagonal prism and pyramid like zinc oxide crystal is attributed to the difference in the growth velocities of various crystal phases. The growth velocities under hydrothermal conditions along the different directions are known to follow the pattern $V(0001) > V(1011) > V(1010)$ [22, 23]. The relative growth rate of these crystal faces will determine the final stage and aspect ratio of the ZNS and the preferential growth along the (0001) polar.

Various nanostructures obtained for the different pH values experimented with are as depicted in Fig. 4(a)–(d). Electron microscopy images were taken with the aid of *Philips XL 830*. Figure 4(e) shows a TEM image of single ZnO nanorods. At pH 8, flake like nanostructures were obtained. This particular structure has more surface area and a very high aspect ratio. The formation of large number of flake like morphologies and a very little growth on the axial growth direction of ZnO indicates the rapid formation of large number of spurious nuclei i.e. $Zn(OH)_2$, and comparatively lesser constituents of growth units $[Zn(OH)_4]^{2-}$ which are responsible for growth. Hexagonal rods with tapered tip are formed when the solution pH was 10. The faster the growth on a plane the sooner the plane disappears. So, the tapering feature insists that the growth along the *c*-axis i.e. along (0001) direction is very much faster than the other faces. The faster growth makes evident the rapid production of $[Zn(OH)_4]^{2-}$ units by the internal heating by microwave irradiation. By changing the pH of the solution with a higher volume of the mineraliser—ammonia in this case—has favoured the production of the growth units ($[Zn(OH)_4]^{2-}$) of ZnO in large volume [24]. However, the opposite face of this is a slow growing phase and so, the other end of the rods is maintained flat [25]. At higher pH well-defined hexagonal rod like morphologies are obtained. The schematics of the specific growth conditions favoured by the effect of pH are illustrated in Fig. 5. In order to compare the growth and size variations i.e., the diameter of the hexagonal nanorods against the percentage of number of particles viewed from SEM are plotted as a histogram. Figures 6(a) and 6(b) show the histograms illustrating the various diameters of the nanorods. For the pH 12 case there is a higher number of size distributions (9 sizes) ranging from 50 nm to 250 nm, whereas the pH 13.5 case has a smaller number of sizes (6 sizes) in the range from 100 nm to 350 nm. The pH 12 has produced a higher number of particles in the diameter range of 125 nm and 200 nm, whereas for the 13.5 case, more particles are in the diameter range of 300 nm and the least number of particles in the 100 nm. For the cases of pH 8 and 10, the SEM images, obtained are un-geometrical, and therefore, it is not easily measurable manually. They may give rise to more errors, and hence they are not illustrated in detail.

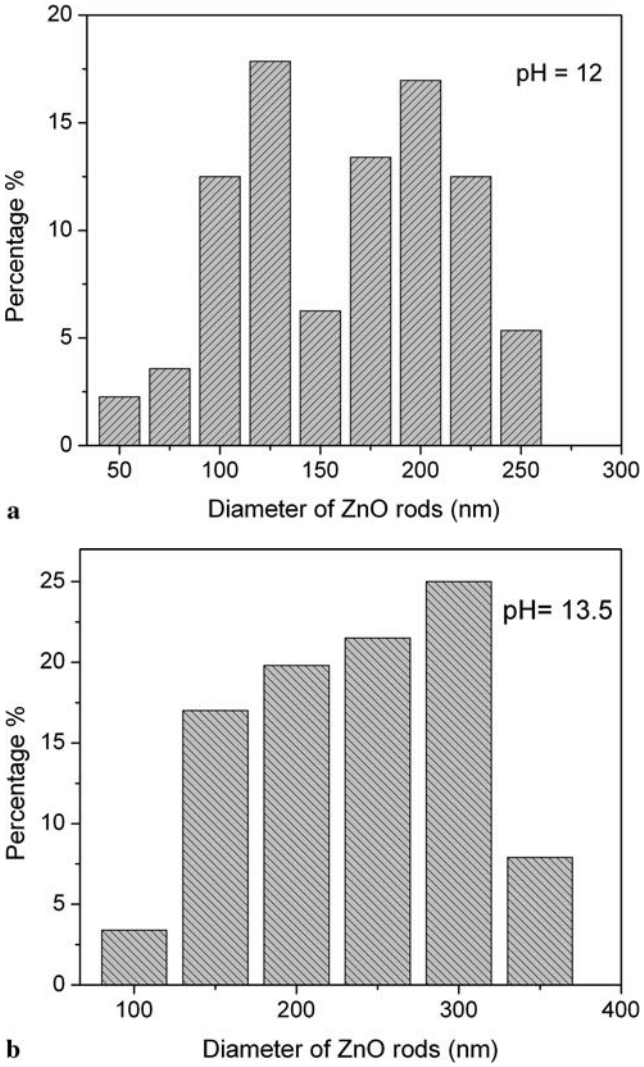


**Fig. 6** Histograms illustrating the difference in size distributions of hexagonal rods produced (**a**) 12, (**b**) 13.5

It is suspected that the secondary growth called Ostwald ripening is more pronounced in this. The growth of the bigger particles at the cost of the smaller ones is known as Ostwald's ripening process [26]. Since the growth units are in smaller numbers, the histogram can depict more size distributions with a lesser rod diameter. But when the pH is 13.5, this favours a smaller number of zinc hydroxide and a larger number of zinc metal ion complexes, the growth units which are responsible for the growth [24]. This is evident in the histogram of Fig. 6(b).

## 4 Conclusions

Rapid microwave assisted one step syntheses of ZnO nanostructures of different morphologies were produced from the solutions of different pH values as is demonstrated. The pre-

pared nanostructures are found to be well crystalline, hexagonal wurtzite structured ZnO. Their mean grain sizes and strains were calculated by using the Scherrer formula and the Williamson–Hall method, respectively. The grain sizes and strains show a pH dependent variation and an inverse relation. The morphology of the obtained nanostructures are seen from the SEM are compared and found to be different for different pH conditions. The reasons for the formation of different morphologies, based on the growth kinetics, are explained schematically. The size distribution histogram has confirmed the phenomenon.

## References


1. U. Ozgar, Y.I. Alivov, C. Liu, A. Teke, M.A. Reshchikov, S. Dogan, V. Avrutin, S.J. Cho, H. Morkoc, J. Appl. Phys. **98**, 041301 (2005)
2. D.C. Look, Mater. Sci. Eng. B **80**, 383 (2001)
3. T. Zhang, W. Dong, M.K. Brewer, S. Konar, R.N. Njabon, Z.R. Tian, J. Am. Chem. Soc. **128**, 10960 (2006)
4. W. Bai, K. Yu, Q. Zhang, F. Xu, D. Peng, Z. Zhu, Mater. Lett. **61**, 3469 (2007)
5. P.X. Gao, Z.L. Wang, Small. **1**, 945 (2005)
6. Y.P. Gao, C.N. Sisk, L.J. Hope-Weeks, Chem. Mater. **19**, 6007 (2007)
7. Z. Li, A. Geßner, J.P. Richters, J. Kalden, T. Voss, C. Kübel, A. Taubert, Adv. Mater. **17**, 951 (2005)
8. C. Jiang, W. Zhang, G. Zou, W. Yu, Y. Qian, J. Phys. Chem. B **109**, 1361 (2005)
9. X. Gao, X. Li, W. Yu, J. Phys. Chem. B **109**, 1155 (2005)
10. Y. Sun, D.J. Riley, M.N.R. Ashfold, J. Phys. Chem. B **110**, 15186 (2006)
11. S. Erten-Ela, S. Cogal, S. Icli, Inorg. Chim. Acta. **362**, 1855 (2009)
12. X. Chu, T. Chen, W. Zhang, B. Zheng, H. Shui, Sensors. Actuat. B, Chem. **142**, 49 (2009)
13. W.W. Wang, Y.J. Zhu, Inorg. Chem. Commun. **7**, 1003 (2004)
14. O.C. Kappe, Angew. Chem., Int. Ed. **43**, 6250 (2004)
15. O.C. Kappe, Chem. Soc. Rev. **37**, 1127 (2008)
16. L. Vayssieres, Adv. Mater. **15**, 464 (2003)
17. V.K. Ivanov, A.S. Shaporev, F.Y. Sharikov, A.Y. Baranchikov, Superlattices Microstruct. **42**, 421 (2007)
18. S. Komarneri, M. Bruno, E. Mariani, Mater. Res. Bull. **35**, 1843 (2000)
19. T. Sekiguchi, S. Miyashita, K. Obara, T. Shishido, N. Sakagami, J. Cryst. Growth. **214**, 72 (2000)
20. B.D. Cullity, *Elements of X-Ray Diffraction* (Addison-Wesley, Reading, 1978)
21. X. Li, Y. Qu, G. Sun, D. Jiang, X. Ouyang, J. Phys. Chem. Solids **68**, 2405 (2007)
22. Z. Zhang, J. Mu, J. Colloid. Interface Sci. **307**, 79 (2007)
23. S. Baruah, J. Dutta, Sci. Technol. Adv. Mater. **10**, 013001 (2009)
24. H. Zhang, D. Yang, Y. Ji, X. Ma, J. Xu, D. Que, Nanotechnology **15**, 622 (2004)
25. L. Vayssieres, Int. J. Nanotechnology **1**, 1 (2004)
26. H. Zhang, D. Yang, Y. Ji, X. Ma, J. Xu, D. Que, J. Phys. Chem. B **108**, 3955 (2004)